Article

Anthropogenic Heat Emissions and Energy Use in Buildings at the Block Scale: Differences across Local Climate Zones and Component Contributions

Yuan Chen, Xilian Luo, and Yupeng Wang *

School of Human Settlements and Civil Engineering, Xi'an Jiaotong University, Xi'an 710049, China
* Correspondence: wang-yupeng@xjtu.edu.cn
Received: 15 October 2025; Revised: 22 December 2025; Accepted: 23 December 2025; Published: 24 December 2025

Abstract: Under global warming and rapid urbanization, anthropogenic heat emission from buildings (AHEb) has become a key driver of urban thermal environments. However, most studies approximate AHEb using building energy consumption, which limits the accurate representation of block-scale heat release and its variability across urban forms. This study examines typical urban blocks representing different Local Climate Zone (LCZ) types in Xi'an, China. Using building energy simulations, we quantify the spatiotemporal characteristics of AHEb and their component mechanisms across LCZs. Results show that in summer, compact high-density blocks (LCZ 1–2) exhibit daily mean heat emission intensities of 134.2–230.0 W/m^2, significantly higher than those of open blocks (LCZ 4–6-II; 72.7–202.7 W/m^2). Peak heat emissions lag solar radiation by approximately 3 h and are 1.7–4.5 times higher than building energy use intensity. In winter, overall heat emissions decrease markedly, with peak values of 101.5–243.9 W/m^2 in compact blocks and 39.4–98.3 W/m^2 in open blocks, while inter-block differences are more strongly influenced by dominant building functions. Component analysis indicates that in summer, HVAC systems and building envelopes contribute 43–68% and 17–53% of total heat emissions, respectively. In winter, relief air dominates heat emissions in commercial and office blocks (29–80%), whereas residential blocks are mainly governed by envelope heat release and air infiltration. These findings demonstrate that equating building energy consumption with heat emissions substantially underestimates actual urban heat release. Integrating the LCZ framework enables more refined and function-sensitive assessments of urban thermal environments.

Keywords: building heat emission; building energy model; local climate zone

1. Introduction

More than 50% of the world's population currently resides in urban areas, a proportion projected to increase to 68% by 2050 [1]. To accommodate rapid population concentration, urban development has increasingly adopted high-density and vertically intensive forms, which have profoundly altered urban canopy structures, land-cover patterns, surface thermal properties, and levels of anthropogenic heat release. These changes reshape near-surface wind fields, radiative processes, and surface energy balances, thereby giving rise to a range of urban climate and environmental problems [2,3]. Among them, the deterioration of the urban thermal environment is particularly prominent and is typically manifested as the urban heat island effect, whereby air temperatures in urban areas can exceed those in surrounding rural regions by up to 10 °C [4]. The persistent intensification of urban heat further exacerbates human heat exposure and health risks [1] and poses growing challenges to energy supply and demand security [5]. Under future climate change scenarios, the extent and severity of these impacts are expected to increase further.

Urban climate is strongly regulated by the built environment. Previous studies have shown that urban climate formation is a complex process jointly driven by multiple built-environment factors, including urban morphology, land cover, surface materials, and anthropogenic activities [6]. In comparison with other factors, however, the role of anthropogenic heat has received relatively limited systematic investigation.

Anthropogenic heat plays a critical role in the urban surface energy balance and urban climate dynamics [7]. Observational and modeling studies have shown that anthropogenic heat increases daytime urban heat island intensity by approximately 1.3 °C in Tokyo and 0.9 °C in Osaka [8], while in Beijing and Shanghai, the correlation coefficients between anthropogenic heat and air temperature exceed 0.7 [9]. Anthropogenic heat emissions are

generally categorized into three major sources: buildings (residential, commercial, and industrial), transportation, and human metabolism [10]. Among these, anthropogenic heat emissions from buildings (AHEbs)—defined as the heat released to the urban atmosphere from building operations, including space conditioning, equipment use, and associated energy dissipation—contribute the largest share, accounting for 50–60% of total anthropogenic heat [11], and up to 83% in commercial districts [12].

Three main approaches are commonly used to estimate AHEbs: inventory-based methods, energy-balance methods, and building energy simulations. Inventory-based methods rely on statistical data such as population density and electricity or gas consumption and are primarily applied at global or regional scales [13], especially in early large-scale assessments. Energy-balance methods estimate AHEbs based on surface energy balance equations across different spatial scales [14]. However, conventional building energy models typically focus on internal heat sources such as heating, ventilation, and air-conditioning (HVAC) systems, while convective and radiative heat release from building envelopes is often insufficiently represented or neglected.

To assess AHEbs at finer spatial scales, physics-based numerical modeling approaches have been widely adopted, including urban canopy meteorological models and building energy models. Urban canopy models generally simplify building energy representations and are mainly applied at the mesoscale and city scales [15]. In contrast, building energy models provide more detailed descriptions of building envelopes, operational schedules, HVAC systems, and occupant activities. Commonly used tools include ANSYS Fluent, DOE-2, and EnergyPlus [16]. Nevertheless, most of these tools primarily account for internal heat sources (e.g., HVAC systems) and typically neglect radiative heat release from building envelopes, as this component does not directly affect conventional building energy performance metrics.

In recent years, EnergyPlus version 9.2 has incorporated a physics-based heat balance radiation model [17], enabling the simulation of multiple building heat emission pathways, including building envelopes, air infiltration, and HVAC systems. Using this approach, several studies have provided more comprehensive assessments of building heat emissions. Ferrando [18] reported significant discrepancies between AHEbs and building energy use. Alhazmi [19] showed that under peak solar irradiance of 972 W/m^2, heat emissions from a six-story office building reached 855 W/m^2, approximately 2–4 times higher than its energy use intensity. Further, Chen et al. [20] demonstrated that HVAC systems and building envelopes accounted for 56% and 24% of total AHEbs, respectively. These findings indicate that estimating AHEbs solely based on heating and cooling energy consumption may lead to substantial underestimation.

To characterize the spatiotemporal variability of urban climate within cities, Stewart and Oke proposed the Local Climate Zone (LCZ) framework [6]. Based on climate-relevant built-environment attributes such as building height, density, and vegetation cover, LCZs classify urban space into 17 types, including 10 built-up and 7 natural land-cover classes. Areas belonging to the same LCZ type typically exhibit similar thermal characteristics, such as land surface temperature and near-surface air temperature. Over the past decade, the LCZ framework has been validated in more than 280 cities worldwide and has been gradually applied in urban planning practices in cities such as Colombo, Toulouse, and Szeged [21]. However, existing studies have mainly focused on morphological and thermal differences among LCZ types, while quantitative comparisons of building heat emission fluxes at the block scale across different LCZs remain limited.

In summary, under the background of global climate warming, accurately quantifying the spatiotemporal characteristics of urban AHEbs is essential for understanding their role in shaping urban climate. Nevertheless, previous studies have largely focused on individual buildings or isolated cases, lacking systematic comparisons of AHEbs at the block scale across different LCZ types. To address this gap, the present study disaggregates AHEbs into three pathways—radiative and convective release from building envelopes, HVAC system heat emissions, and active/passive air infiltration—and integrates them within the LCZ framework to quantitatively evaluate AHEbs across different LCZ-based urban blocks and compare them with building energy use intensity. Taking representative blocks of different LCZ types in Xi'an, China, as case studies, this work systematically analyzes the composition and relative contributions of AHEbs, providing scientific support for climate-adaptive urban planning and building energy-efficiency strategies.

2. Method

2.1. Research Area and Selection of Sample Blocks

Xi'an is one of China's major metropolitan cities and serves as a regional hub that attracts a large population from northwestern provinces, resulting in characteristically high urban development intensity. As shown in Figure 1, Xi'an is located in the Guanzhong Plain near the geographical center of China (34.3416° N, 108.9398° E). The city lies in a climatic transition zone between a temperate semi-humid monsoon climate and a semi-arid climate.

According to the Köppen–Geiger climate classification, Xi'an is categorized as Cwa (humid subtropical climate with dry winters). With rapid urban expansion, the urban heat island effect in Xi'an has intensified in recent decades, with the heat island area increasing by a factor of approximately 2.4 between 2000 and 2020 and the maximum UHI intensity reaching 7.3 °C [22].

The central urban area of Xi'an, defined as the area within the Third Ring Road, was selected as the study area, covering approximately 350 km^2. This area represents the city's most densely populated and highly built-up zone. As illustrated in Figure 1, its spatial structure follows a monocentric concentric-ring pattern, consisting of the inner city within the First Ring Road (city wall), the Second Ring Road zone, and the Third Ring Road zone. The central area exhibits highly diverse urban morphologies, including both historical conservation districts and high-intensity development zones. Except for large industrial parks, it encompasses nearly all major urban land-cover and surface types.

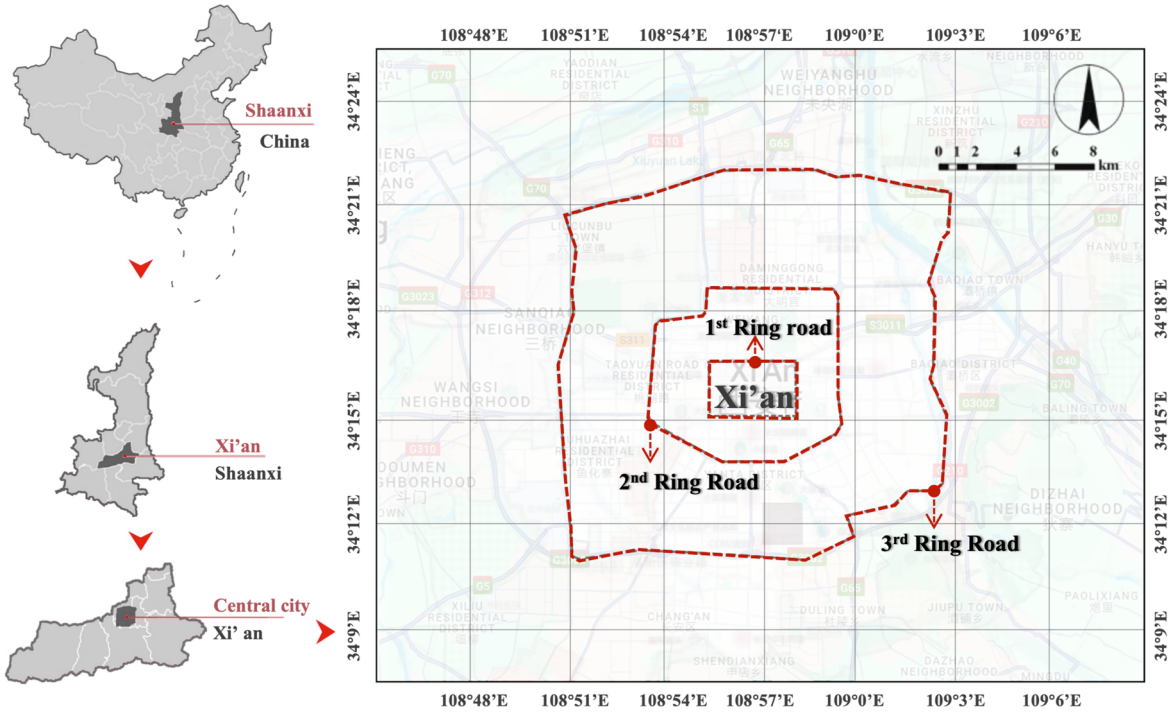

Figure 1. Location and spatial structure of the central urban area of Xi'an.

Within the First Ring Road, the historic inner city is subject to strict heritage conservation regulations, resulting in a distinctive urban form characterized by high building density and medium building height, and exhibiting the poorest thermal environmental conditions [23]. Previous studies have shown that compact urban blocks are typically priority targets for evaluation and optimization in urban renewal initiatives [24–28]. As shown in Figure 2, five representative compact blocks were selected from within the First Ring Road, including three LCZ 2 blocks and two LCZ 1 blocks. These two LCZ types are widely distributed in the historic inner city, where LCZ 1 represents the highest development intensity, and LCZ 2 corresponds to the most prevalent high-density urban form.

In addition, other LCZ types with relatively large areal proportions were selected from outside the First Ring Road. Representative blocks were chosen from the southern inner area of the Third Ring Road, where urban functions and surface types are highly diverse, and multiple dominant LCZ types coexist. Ultimately, five representative blocks corresponding to LCZ 4, LCZ 4-II, and LCZ 5-II—three of the most prevalent LCZ types in Xi'an—were selected. In contrast to LCZ 1 and LCZ 2, these LCZs represent more open urban block configurations. The three-dimensional built-environment characteristics of the selected blocks are illustrated in Figure 2.

In summary, the ten selected blocks cover the most prevalent LCZ types in Xi'an and include major mixed urban functions such as residential, commercial, office, educational, and hotel uses. These blocks not only capture the distinctive characteristics of historical conservation areas, but also represent typical high-intensity development patterns of a megacity. Together, they provide a realistic representation of Xi'an's urban built environment under the combined influences of heritage preservation and rapid urbanization.

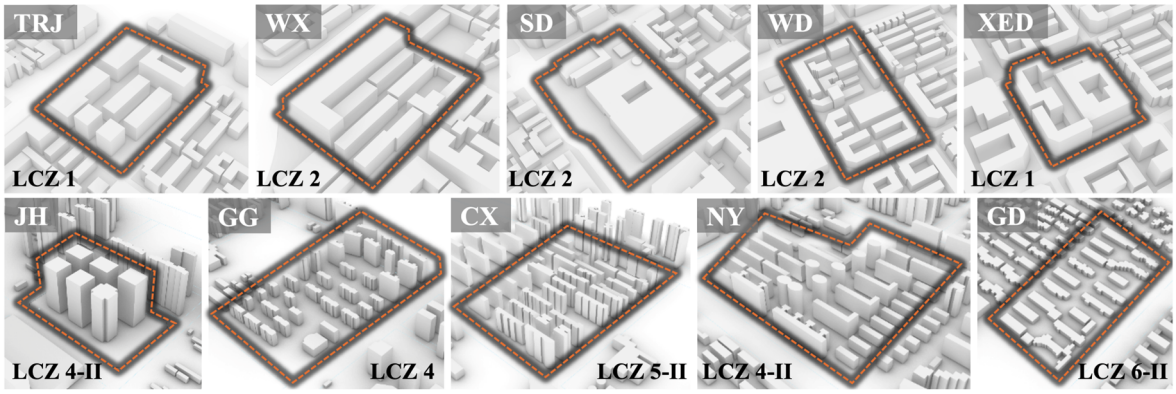

Figure 2. Rhino vector spatial model of typical blocks.

2.2. AHEb Simulation

AHEb fluxes were calculated using a physics-based building energy modeling approach. First, the conceptual components of AHEbs are described, followed by a presentation of the model setup, boundary conditions, thermophysical properties of building envelope materials, and operational settings.

2.2.1. Framework of AHEb

Based on the AHEbs framework implemented in EnergyPlus version 9.2 and later, this study defines AHEbs as the combined heat released to the outdoor environment, air infiltration and exhaust, and HVAC systems, as expressed in Equations (1) and (2).

$$AHEb = AHEb_{Surface} + AHEb_{Zone} + AHEb_{HVACSystem} \quad (1)$$

$$AHEb_{HVACSystem} = AHEb_{HVAC} + AHEb_{ReliefAir} \quad (2)$$

Specifically, $AHEb_{Surface}$ (W/m^2) represents the areal heat emission intensity from building envelope surfaces, including convective heat transfer to the ambient air caused by the temperature difference between exterior surface temperature and outdoor dry-bulb air temperature, as well as longwave radiation absorbed by atmospheric water vapor and particulate matter. Radiative heat exchange emitted toward surrounding surfaces (e.g., adjacent buildings, trees, the sky, and ground surfaces) is not included, as this portion does not directly heat the surrounding air. $AHEb_{Zone}$ (W/m^2) denotes the heat emission intensity associated with active and passive air exchange between indoor and outdoor environments, including air leakage through openings (e.g., windows and doors), uncontrolled exfiltration through envelope cracks, and mechanically exhausted air from kitchens or bathrooms. $AHEb_{HVACSystem}$ (W/m^2) refers to the total heat rejection from HVAC systems per unit area, which consists of two components: $AHEb_{HVAC}$ (W/m^2), representing waste heat released by condensers, and $AHEb_{ReliefAir}$ (W/m^2), representing heat exchange associated with relief air discharged from air handling units.

2.2.2. Simulation Setup

Building energy models for the ten representative urban blocks were developed on the Grasshopper platform using Ladybug Tools version, including Honeybee and Dragonfly. During model construction, the influence of adjacent blocks—particularly buildings along road-facing boundaries—was explicitly considered and incorporated into the simulation domain. $AHEb_{Surface}$ was obtained from the EnergyPlus output variable Surface Outside Face Heat Emission to Air Rate. $AHEb_{Zone}$ was calculated as the sum of Site Total Zone Exfiltration Heat Loss and Site Total Zone Exhaust Air Heat Loss. $AHEb_{HVACSystem}$ was derived from the combined outputs of HVAC System Total Heat Rejection Energy and Air System Relief Air Total Heat Loss Energy. To enable comparison between AHEbs and building energy consumption, the block-level building energy use intensity (EUI_b, W/m^2), representing the intensity of a building's energy demand, was simultaneously extracted from the simulations.

2.2.3. Outdoor Meteorological Boundary Conditions

To more accurately represent building heat emissions under block-specific microclimatic conditions, this study did not adopt air temperature and relative humidity data from suburban reference meteorological stations or typical meteorological year datasets as boundary conditions. Instead, the average air temperature and relative humidity measured at outdoor monitoring points within each block during the observation period were used. In

this study, the summer and winter analyses correspond to two typical days in July and December 2022, respectively. Global solar radiation was obtained from observations at the Xianyang Jinghe National Reference Meteorological Station.

2.2.4. Building Envelope Construction and Thermal Properties

From the late 19th century to the early 21st century, large-scale urban construction in Xi'an predominantly employed reinforced concrete structural systems with masonry infill envelopes. The selected representative blocks were developed within this period. To reduce excessive variability in numerical simulations and to focus on the core research objectives, uniform opaque envelope materials and construction assemblies were applied to all buildings across the study blocks. Envelope thermal properties were determined based on Xi'an's climatic zoning and relevant engineering standards. Specifically, building envelope characteristics were defined according to [29] and [30], while construction details were specified following [31]. Detailed parameters are summarized in Tables 1–4.

Table 1. Building window-to-wall ratio and HVAC parameters of the blocks.

Function	Window-to-Wall Ratio	HVAC System	Performance Coefficient
Residential	North: 0.3; South: 0.5	Split AC: VRF	2.8 [32]
Commercial	0.4	VAV Air-Cooled chiller with central air source heat pump reheat	3.0
Office	0.4		
Hotel	0.4		

Table 2. Thermal properties and construction parameters of opaque envelope materials.

	Thermal Conductivity (W/m·K)	Density (kg/m^3)	Specific Heat Capacity (J/kg·K)
Porous brick (PB)	0.44	1180	1050
Reinforce concrete (RC)	1.74	2500	920
Reinforce concrete (EPS)	0.047	100	1380
Gravel concrete (GC)	1.28	2100	920
Lime mortar (LM)	0.81	1600	1050
Plywood slab (PS)	0.17	600	2510

Table 3. Thermal properties and construction parameters of opaque envelope materials.

Opaque Envelope Construction	
Exterior wall	40 mm EPS + 240 mm PB + 14 mm LM
Ceiling	15 mm PS + 100 mm RC
Roof	40 mm GC + 90 mm EPS + 100 mm RC

Table 4. Thermal properties of transparent envelope materials.

Heat Transfer Coefficient /W/m^2·K	SHGC	Solar Radiation Absorbed Factor	Reflectance Factor	Long Wavelength Radiation Factor
2.3	0.34	0.7	0.3	0.95

2.2.5. Building Operational Settings

Significant differences in operational characteristics among buildings with different functions lead to pronounced variability in building anthropogenic heat emissions. Operational parameters related to occupants, lighting, and equipment were defined according to [31]. Figures 3 and 4, together with Table 5, summarize key operational parameters for the representative cases, including occupant density, lighting power density, equipment usage rates, ventilation rates, and HVAC set-point temperatures for different building functions.

Table 5. Operation program settings for different functional buildings.

	Commercial	Residential	Official	Hotel
Personnel density (m^2/person)	4	36	8	30
Personnel activity (W/ person)	181	120	134	108
Lighting intensity (W/m^2)	10	5	9	7
Equipment intensity (W/m^2)	13	4	15	15
Ventilation intensity (ACH)	1.1	0.5	1	0.5
Flow per person (m^3/s·person)	0.005	0.033	0.0083	0.0083

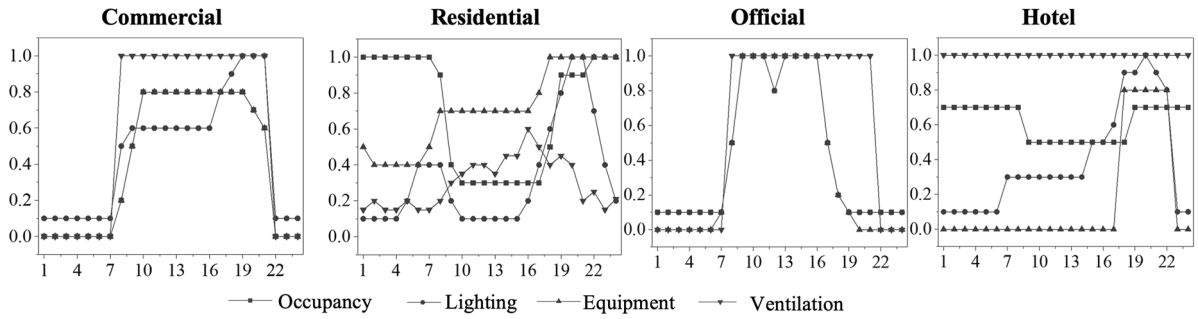

Figure 3. Operational parameters of different building types.

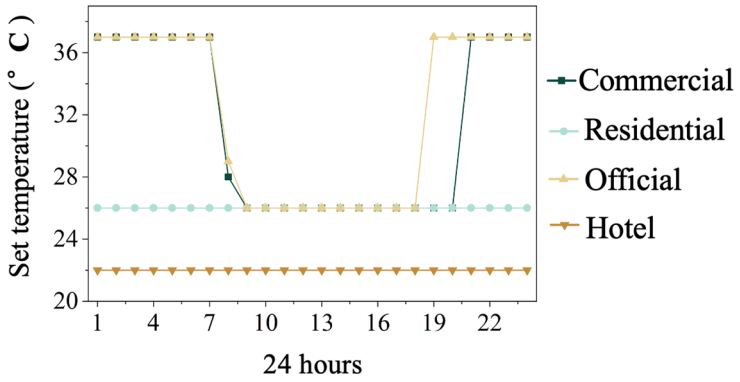

Figure 4. HVAC temperature and ventilation settings.

3. Results and Discussion

3.1. AHEbs across Different LCZ Blocks

3.1.1. Summer

Figure 5 illustrates the spatial distribution of daily mean AHEb intensity across the representative blocks during summer. Pronounced inter-block differences in building heat fluxes are observed among different Local Climate Zone (LCZ) types. Compact blocks classified as LCZ 1–2 exhibit AHEbs values ranging from 134.2 to 230.0 W/m^2, which are generally higher than those of open blocks (LCZ 4–6-II), whose AHEbs range from 72.7 to 202.7 W/m^2. Exceptions are observed for blocks XED and JH, primarily attributable to differences in dominant building functions. Although XED belongs to the most compact LCZ type (LCZ 1), its dominant hotel function results in substantially lower heat emissions than those of commercial and office blocks. Conversely, JH is classified as an open-type block (LCZ 4-II), yet its nearly 90 m building height and office-dominated function lead to significantly higher AHEbs than those of the other four open residential blocks. These results indicate that even within the same LCZ type, variations in dominant building function can lead to substantial differences in block-scale building heat emissions.

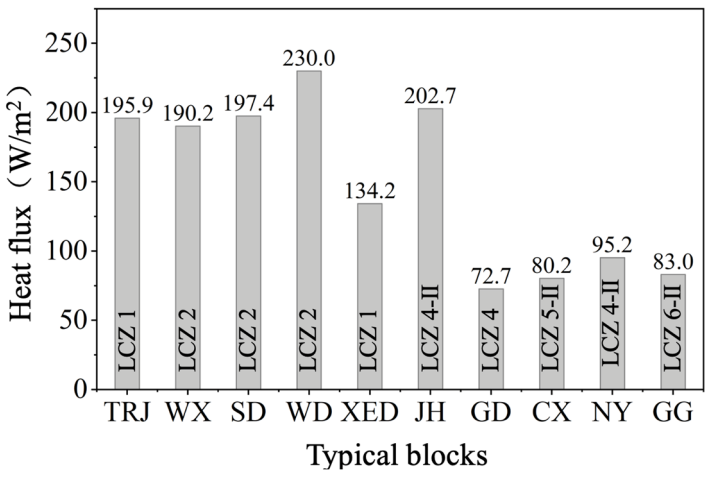

Figure 5. Daily mean AHEb flux of typical blocks in summer.

At a finer temporal scale, the diurnal dynamics of summer building heat emissions were further examined. Figure 6 presents the hourly variations in AHEb, EUI_b, and background global solar radiation for all blocks. Global solar radiation peaks at approximately 13:00, reaching up to 979 W/m^2. The AHEb peak lags behind the solar radiation peak by approximately 3 h. For compact blocks (LCZ 1–2), peak AHEb ranges from 284 to 513 W/m^2, whereas open blocks (LCZ 4–6-II) exhibit significantly lower peaks of 178 to 315 W/m^2. The EUI_b peak occurs approximately 5 h after the solar radiation peak, with values ranging from 113 to 145 W/m^2. Notably, AHEb substantially exceeds EUI_b across all blocks, by approximately 1.7 to 4.5 times. This finding is consistent with results from regions of the United States with similar Köppen climate classifications (Cfa), such as a case study of a six-story office building in which the actual peak building heat emission was four times greater than the energy consumption [19]. These results demonstrate that equating building energy consumption with building heat emissions leads to a severe underestimation of actual anthropogenic heat release.

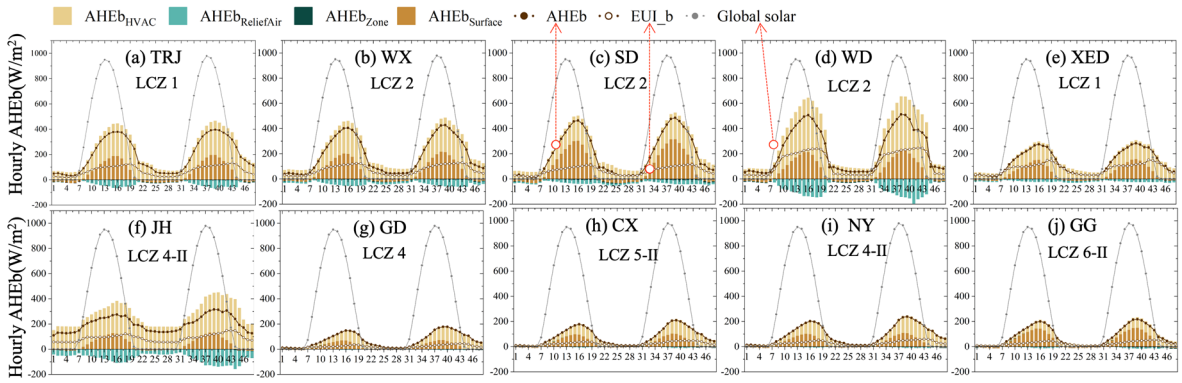

Figure 6. Hourly variations of AHEb flux in summer blocks.

3.1.2. Winter

Figure 7 shows the wintertime AHEb levels for the representative blocks. Overall, winter AHEb values are significantly lower than those in summer. For compact blocks (LCZ 1–2), AHEb ranges from 9.4 to 85.0 W/m^2, with block WD exhibiting substantially higher values than the others. Open blocks (LCZ 4–6-II) generally show lower AHEb levels than compact blocks, although JH again stands out with significantly higher emissions than the other open blocks. Importantly, notable differences in AHEbs are observed within the same LCZ type, primarily attributable to commercial- and office-dominated functions. Compared with summer, winter AHEb is more strongly influenced by dominant building function. The four open blocks dominated by residential use exhibit the lowest building heat emissions, with AHEb values for GD, CX, and NY approaching zero.

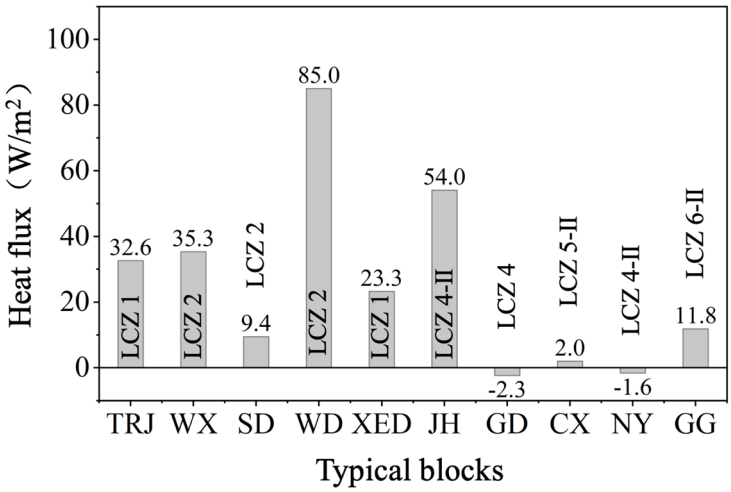

Figure 7. Block-scale mean AHEb flux in winter.

Figure 8 presents the diurnal variations in winter AHEb, EUI_b, and global solar radiation. The peak global solar radiation reaches 509.3 W/m^2, approximately half of the summer peak value. The AHEb peak lags behind the solar radiation peak by about 2 h. Peak AHEb values for compact blocks range from 101.5 to 243.9 W/m^2, while open blocks exhibit much lower peaks of 39.4 to 98.3 W/m^2, consistent with summer patterns. Peak EUI_b

values range from 25.1 to 133.9 W/m^2. Unlike summer, EUI_b exceeds AHEb during the daytime period between 08:00 and 13:00 (from sunrise to peak solar radiation). This indicates that wintertime building heat emissions depend strongly on solar radiation, with shortwave solar gains absorbed by building envelopes and subsequently released to the outdoor environment.

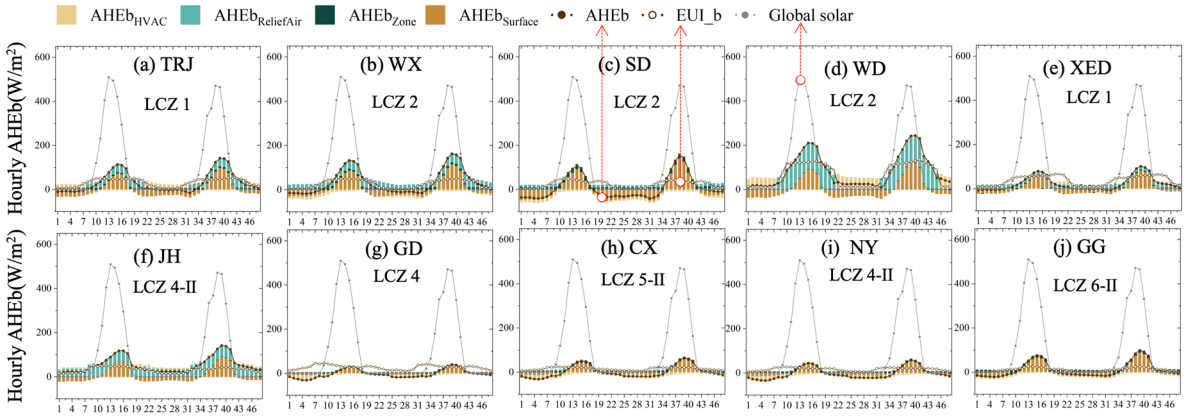

Figure 8. Hourly variations of AHEb flux in winter blocks.

3.2. Composition of AHEbs across LCZ Blocks

3.2.1. Summer

Figure 9a presents the heat fluxes of different building heat emission components. AHEb$_{HVAC}$ is the dominant contributor across all block types, particularly in the commercial and office blocks WD and JH, where values reach 229.9 and 231.0 W/m^2, respectively. Despite belonging to different LCZ types, these two blocks exhibit similar HVAC-related heat emissions, indicating that functional type and development intensity can result in comparable AHEb$_{HVAC}$ levels across different LCZs. The second largest component is AHEb$_{Surface}$, with daily mean values ranging from 23.1–88.4 W/m^2. In compact blocks (LCZ 1–2), AHEb$_{HVAC}$ is substantially higher than AHEb$_{Surface}$. In contrast, in open blocks (LCZ 4–6-II), the two components are comparable, and in the low-rise LCZ 6-II blocks, AHEb$_{Surface}$ even exceeds AHEb$_{Surface}$. This indicates that envelope-related heat emissions play a role nearly as important as HVAC emissions in open blocks. Consequently, equating HVAC heat rejection with total building heat emissions leads to significant underestimation, particularly for LCZ 4–6 blocks.

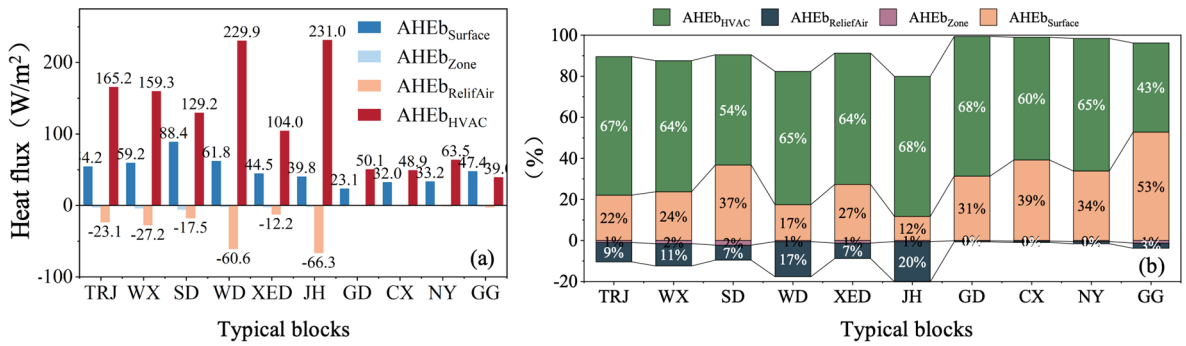

Figure 9. Four components of AHEb in summer: (**a**) fluxes and (**b**) proportions.

Figure 9b further illustrates the proportional contributions of the four components. AHEb$_{HVAC}$ dominates, accounting for 54–68% in nine medium- and high-rise blocks, except for the low-rise LCZ 6-II block, where it contributes only 43%. AHEb$_{Surface}$ accounts for 17–53% and consistently represents a positive heat source to the surrounding air. In contrast, AHEb$_{ReliefAir}$ and AHEb$_{Zone}$ contribute minimally and negatively. Relief air contributions are highest in the commercial complex WD and the high-rise office block JH, at 17% and 20%, respectively. Notably, GG (LCZ 6-II) is the only block where AHEb$_{Surface}$ (53%) exceeds AHEb$_{HVAC}$ (43%), owing to its high building density, large envelope surface area, and relatively low HVAC intensity.

Overall, in summer, HVAC systems dominate building heat emissions in high-rise and high-density blocks, whereas envelope-related heat emissions play a leading role in open blocks. These findings demonstrate that the dominant building heat emission pathways vary with block density, height, and function.

3.2.2. Winter

Figure 10a shows the wintertime heat fluxes of different AHEb components, all of which are substantially lower than their summer counterparts. Unlike summer, $AHEb_{HVAC}$ is no longer the dominant component. In the six blocks containing significant commercial functions (TRJ–JH), $AHE_{ReliefAir}$ contributes the most, with WD and JH reaching 58.2 and 43.1 W/m^2, respectively. For the four residential blocks (GD, CX, NY, and GG), $AHEb_{Zone}$ dominates. Among them, GG exhibits significantly higher AHEb than the other three residential blocks because its low-rise buildings have limited HVAC heat losses, allowing envelope and infiltration-related heat emissions to dominate and remain positive. In contrast, for the other three residential blocks, heat gains and losses from different components largely offset each other, consistent with findings from similar climatic regions [17].

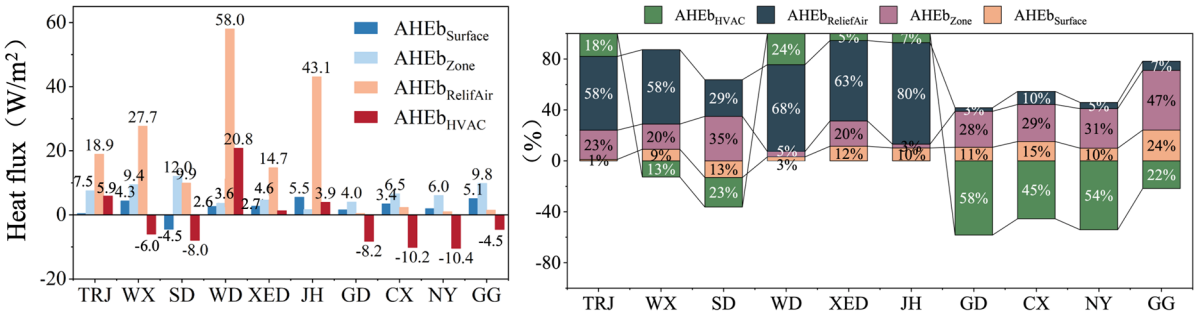

Figure 10. Four components of AHEb in winter: (**a**) fluxes and (**b**) proportions.

Figure 10b presents the proportional contributions of winter building heat emission components. In contrast to the summer dominance of $AHEb_{HVAC}$, winter emissions are mainly governed by $AHE_{ReliefAir}$ and $AHEb_{Zone}$. In commercial and office-dominated blocks, $AHE_{ReliefAir}$ accounts for 29–80% of total emissions. In residential blocks, different components nearly cancel each other, except for GG (LCZ 6-II), where winter building heat emissions are dominated by $AHEb_{Zone}$ and $AHEb_{Surface}$, resulting in net heat release to the ambient air.

Overall, in winter, the contributions of different building heat emission components vary substantially with dominant building function. Public-service-dominated blocks should primarily focus on relief air emissions, whereas residential blocks require attention to envelope- and infiltration-related heat emissions. This further indicates that the key building heat emission pathways differ across LCZ types and seasons.

4. Conclusions

This study systematically quantitatively analyzed the spatial variability, diurnal dynamics, and compositional mechanisms of AHEb across representative blocks of different LCZ types in Xi'an, China. The results demonstrate clear and systematic differences in AHEb across LCZ types, seasons, and dominant building functions, with actual heat emissions substantially exceeding traditional estimates based on building energy consumption alone.

In summer, compact high-density blocks (LCZ 1–2) consistently exhibit significantly higher AHEb than open blocks (LCZ 4–6-II). However, even within the same LCZ type, variations in dominant building function can cause substantial variability, indicating that LCZ morphological characteristics alone are insufficient to fully capture block-scale AHEb. At the diurnal scale, AHEb peaks systematically lag behind solar radiation peaks and are typically several times higher than EUI_b, highlighting the risk of substantial underestimation when energy consumption is used as a proxy for heat emissions.

In winter, overall heat emissions are markedly lower than in summer, and inter-block differences are more strongly controlled by dominant building function rather than LCZ morphology. Commercial and office blocks maintain relatively high heat emissions, whereas residential blocks exhibit much lower levels, with heat gains and losses partially or nearly offsetting each other in some cases. During daytime hours, wintertime heat emissions show a stronger dependence on solar radiation, with envelope-mediated heat release becoming a key mechanism, leading to periods when EUI_b temporarily exceeds AHEb.

From a mechanistic perspective, the dominant pathways of AHEb vary substantially across LCZ types and seasons. HVAC systems dominate summer heat emissions in high-rise and high-density blocks, whereas envelope-related emissions are equally important or dominant in open, low-rise blocks. In winter, relief air emissions govern AHEb in commercial and office blocks, while envelope and infiltration processes dominate in residential blocks. These findings indicate that different LCZ types require function- and season-specific attention to distinct heat emission components.

This study reveals pronounced block-scale heterogeneity and strong seasonal modulation of building anthropogenic heat emissions, underscoring the necessity of explicitly distinguishing building heat emissions from building energy consumption. Integrating the LCZ framework with a detailed decomposition of building heat emission pathways enhances the realism of urban climate simulations and provides a scientific basis for developing targeted, LCZ-specific, and seasonally adaptive strategies for urban heat mitigation and building energy efficiency.

Author Contributions: Y.C.: Writing—original draft, Investigation, Formal analysis; Y.W.: Writing—review & editing, Resources, Funding acquisition, Conceptualization; X.L.: Validation, Supervision, Resources. All authors have read and agreed to the published version of the manuscript.

Funding: This study was funded by the National Natural Science Foundation of China (grant number 52350610262).

Institutional Review Board Statement: Not applicable.

Informed Consent Statement: Not applicable.

Data Availability Statement: Not applicable.

Conflicts of Interest: Given the role as Editorial Board Member of Green Energy and Fuel Research, Yupeng Wang had no involvement in the peer review of this paper and had no access to information regarding its peer-review process. Full responsibility for the editorial process of this paper was delegated to another editor of the journal. The authors declare no conflict of interest.

Use of AI and AI-Assisted Technologies: No AI tools were utilized for this paper.

References

1. United Nations Department of Economic and Social Affairs. *World Urbanization Prospects 2018*: *Highlights*; United Nations: New York, NY, USA, 2019.
2. Soon, W.W.-H.; Connolly, R.; Connolly, M. Comparing the Current and Early 20th Century Warm Periods in China. *Earth-Sci. Rev.* **2018**, *185*, 80–101.
3. Yan, X.; Luo, X.; Wang, Y. Integrating Environmental and Energy Justice into Climate-Adaptive Urban Planning: A Systematic Review. *Green Energy Fuel Res.* **2025**, *2*, 293–302.
4. Oke, T.R.; Mills, G.; Christen, A.; et al. *Urban Climates*; Cambridge University Press: Cambridge, UK, 2017.
5. Wang, H.; Yang, J.; Chen, G.; et al. Machine Learning Applications on Air Temperature Prediction in the Urban Canopy Layer: A Critical Review of 2011–2022. *Urban Clim.* **2023**, *49*, 101499.
6. Stewart, I.D.; Oke, T.R. Local Climate Zones for Urban Temperature Studies. *Bull. Am. Meteorol. Soc.* **2012**, *93*, 1879–1900.
7. Vahmani, P.; Luo, X.; Jones, A.; et al. Anthropogenic Heating of the Urban Environment: An Investigation of Feedback Dynamics between Urban Micro-Climate and Decomposed Anthropogenic Heating from Buildings. *Build. Environ.* **2022**, *213*, 108841.
8. Kikegawa, Y.; Tanaka, A.; Ohashi, Y.; et al. Observed and Simulated Sensitivities of Summertime Urban Surface Air Temperatures to Anthropogenic Heat in Downtown Areas of Two Japanese Major Cities, Tokyo and Osaka. *Theor. Appl. Climatol.* **2014**, *117*, 175–193.
9. Niu, Q.; Nie, C.Q.; Lin, F.; et al. Model Study of Relationship between Local Temperature and Artificial Heat Release. *Sci. China Technol. Sci.* **2012**, *55*, 821–830.
10. Zheng, Y.; Weng, Q. High Spatial- and Temporal-Resolution Anthropogenic Heat Discharge Estimation in Los Angeles County, California. *J. Environ. Manag.* **2018**, *206*, 1274–1286.
11. Luo, X.; Vahmani, P.; Hong, T.; et al. City-Scale Building Anthropogenic Heating during Heat Waves. *Atmosphere* **2020**, *11*, 1206.
12. Quah, A.K.L.; Roth, M. Diurnal and Weekly Variation of Anthropogenic Heat Emissions in a Tropical City, Singapore. *Atmos. Environ.* **2012**, *46*, 92–103.
13. Lu, Y.; Wang, Q.; Zhang, Y.; et al. An Estimate of Anthropogenic Heat Emissions in China. *Int. J. Climatol.* **2016**, *36*, 1134.
14. Hou, H.; Su, H.; Liu, K.; et al. Driving Forces of UHI Changes in China's Major Cities from the Perspective of Land Surface Energy Balance. *Sci. Total Environ.* **2022**, *829*, 154710.
15. Takane, Y.; Kikegawa, Y.; Hara, M.; et al. A Climatological Validation of Urban Air Temperature and Electricity Demand Simulated by a Regional Climate Model Coupled with an Urban Canopy Model and a Building Energy Model in an Asian Megacity. *Int. J. Climatol.* **2017**, *37*, 1035–1052.
16. Ahmad, M.W.; Mourshed, M.; Yuce, B.; et al. Computational Intelligence Techniques for HVAC Systems: A Review. *Build. Simul.* **2016**, *9*, 359–398.
17. Hong, T.; Ferrando, M.; Luo, X.; et al. Modeling and Analysis of Heat Emissions from Buildings to Ambient Air. *Appl. Energy* **2020**, *277*, 115566.

18. Ferrando, M.; Hong, T.; Causone, F. A Simulation-Based Assessment of Technologies to Reduce Heat Emissions from Buildings. *Build. Environ.* **2021**, *195*, 107772.
19. Alhazmi, M.; Sailor, D.J.; Anand, J. A New Perspective for Understanding Actual Anthropogenic Heat Emissions from Buildings. *Energy Build.* **2022**, *258*, 111860.
20. Chen, W.; Zhou, Y.; Xie, Y.; et al. Estimating Spatial and Temporal Patterns of Urban Building Anthropogenic Heat Using a Bottom-Up City Building Heat Emission Model. *Resour. Conserv. Recycl.* **2022**, *177*, 105996.
21. Yang, J.; Yu, W.; Baklanov, A.; et al. Mainstreaming the Local Climate Zone Framework for Climate-Resilient Cities. *Nat. Commun.* **2025**, *16*, 5705.
22. Liu, Z.N.; Yin, X.J. Urban Heat Island Effect and Meteorologic Factors in Xi'an. *J. Arid Land Resour. Environ.* **2008**, *22*, 87–90.
23. Xu, D.; Zhou, D.; Wang, Y.; et al. Temporal and Spatial Variations of Urban Climate and Derivation of an Urban Climate Map for Xi'an, China. *Sustain. Cities Soc.* **2020**, *52*, 101850.
24. Richard, Y.; Emery, J.; Dudek, J.; et al. How Relevant are Local Climate Zones and Urban Climate Zones for Urban Climate Research? Dijon (France) as a Case Study. *Urban Clim.* **2018**, *26*, 258–274.
25. Zheng, Y.; Ren, C.; Shi, Y.; et al. Mapping the Spatial Distribution of Nocturnal Urban Heat Island Based on Local Climate Zone Framework. *Build. Environ.* **2023**, *234*, 110197.
26. Liu, L.; Lin, Y.; Xiao, Y.; et al. Quantitative Effects of Urban Spatial Characteristics on Outdoor Thermal Comfort Based on the LCZ Scheme. *Build. Environ.* **2018**, *143*, 443–460.
27. Lehnert, M.; Geletič, J.; Dobrovolný, P.; et al. Temperature Differences among Local Climate Zones Established by Mobile Measurements in Two Central European Cities. *Clim. Res.* **2018**, *75*, 53–64.
28. Zheng, Y.; Miao, S.; Li, J.; et al. Climate-Adaptive Neighborhood Planning Strategies for High-Temperature Response in Hong Kong. *Planner* **2024**, *40*, 99–107.
29. *JGJ 26-2018*; Design Standard for Energy Efficiency of Residential Buildings in Severe Cold and Cold Zones. China Architecture & Building Press: Beijing, China, 2018.
30. *GB 50189-2015*; Design Standard for Energy Efficiency of Public Buildings. China Architecture & Building Press: Beijing, China, 2015.
31. *JGJ/T 449-2018*; Standard for Green Performance Calculation of Civil Buildings. China Architecture & Building Press: Beijing, China, 2018.
32. Ge, J.; Wang, Y.; Guo, Y.; et al. Multiple-Scale Urban Form Renewal Strategies for Improving Diffusion of Building Heat Emission—A Case in Xi'an, China. *Energy Build.* **2025**, *328*, 115160.